Paper

SPOT-GPR: A Freeware Tool for Target Detection and Localization in GPR Data Developed within the COST Action TU1208

Simone Meschino[1] and Lara Pajewski[2]

[1] *Airbus Defence and Space, Friedrichshafen, Germany*
[2] *Department of Information Engineering, Electronics and Telecommunications, Sapienza University of Rome, Rome, Italy*

https://doi.org/10.26636/jtit.2017.121017

Abstract—SPOT-GPR (release 1.0) is a new freeware tool implementing an innovative Sub-Array Processing method, for the analysis of Ground-Penetrating Radar (GPR) data with the main purposes of detecting and localizing targets. The software is implemented in Matlab, it has a graphical user interface and a short manual. This work is the outcome of a series of three Short-Term Scientific Missions (STSMs) funded by European COoperation in Science and Technology (COST) and carried out in the framework of the COST Action TU1208 "Civil Engineering Applications of Ground Penetrating Radar" (www.GPRadar.eu). The input of the software is a GPR radargram (B-scan). The radargram is partitioned in sub-radargrams, composed of a few traces (A-scans) each. The multi-frequency information enclosed in each trace is exploited and a set of dominant Directions of Arrival (DoA) of the electromagnetic field is calculated for each sub-radargram. The estimated angles are triangulated, obtaining a pattern of crossings that are condensed around target locations. Such pattern is filtered, in order to remove a noisy background of unwanted crossings, and is then processed by applying a statistical procedure. Finally, the targets are detected and their positions are predicted. For DoA estimation, the MUltiple SIgnal Classification (MUSIC) algorithm is employed, in combination with the matched filter technique. To the best of our knowledge, this is the first time the matched filter technique is used for the processing of GPR data. The software has been tested on GPR synthetic radargrams, calculated by using the finite-difference time-domain simulator gprMax, with very good results.

Keywords—Direction-of-Arrival algorithms, Ground-Penetrating Radar, matched filter technique, MUltiple SIgnal Classification (MUSIC), Sub-Array Processing.

1. Introduction

The identification of cables, pipes, conduits and other utilities buried in the soil or embedded in walls, as well as the localization of reinforced elements in concrete structures, are important tasks in civil engineering and have been extensively studied in the last years. The most commonly used non-destructive testing methods exploit electromagnetic waves – a Ground-Penetrating Radar (GPR) [1], [2] illuminates the area of interest by using a transmitting antenna or a set of sources. The echo is collected by a receiving antenna or a set of sensors, then, the recorded radargrams are processed, in order to extract information about the scenario and localize the sought objects [3]–[6].

SPOT-GPR stands for "Sub-array Processing Open Tool for GPR applications" and is a novel freeware tool that can be used for detecting (spotting) targets in a GPR radargram and for estimating their positions. The tool implements an innovative sub-array processing method, based on the use of smart-antenna and radar techniques. It has a Graphical User Interface (GUI) and a short manual, with examples. It was developed during three European COoperation in Science and Technology (COST) Short-Term Scientific Missions (STSMs), as a contribution to the COST Action TU1208 "Civil Engineering Applications of Ground Penetrating Radar" [7]. Those STSMs were carried out in May 2015 [8], [9], January 2016 [10]–[12], and December 2016 – January 2017 [13], [14].

In applications involving smart antennas and in the presence of several transmitters operating simultaneously, it is important for a receiving array to be able to estimate the Directions of Arrival (DoAs) of the incoming signals, in order to decipher how many emitters are present and predict their positions [15], [16]. A number of methods have been devised for DoA estimation: MUltiple SIgnal Classification (MUSIC) [17] and Estimation of Signal Parameters via Rotational Invariance Technique (ESPRIT) [18] are amongst the most popular ones. When a GPR is used to detect and localize targets in the ground or in a structure, the scenario is similar; hence, analogous techniques can be used for target detection and localization. The electromagnetic sources are the currents induced on the sought targets and DoA algorithms can be used for estimating where the electromagnetic field back-scattered by the targets comes from [19]–[22]. However, there are important differences between smart-antenna and GPR problems, which need to be considered and properly treated:

- In GPR scenarios, targets are embedded in a medium different than the one where the GPR antennas are operating: refraction effects occurring at the interface between the air and the host medium cannot be neglected.
- A GPR radargram (usually denominated B-scan), to be processed for predicting the number of targets and their positions, is a set of traces (A-scans) measured by an antenna in different spatial points. Each trace is a vector of electric-field amplitudes measured in a series of instants, within a suitable time window. After recording a trace in a given spatial point, the GPR is moved to the subsequent point, where a new trace is recorded. In smart-antennas applications, instead, the data to be processed are collected by different antennas, which perform their measurements simultaneously. Inasmuch a GPR scenario usually does not change while a radargram is recorded, this difference is not important. The radargram can be treated as if the A-scans were recorded by an array of identical antennas performing simultaneous measurements.
- DoA algorithms assume that the electromagnetic sources are in the far-field region of the receiving array, hence the wavefront illuminating the array can be considered as planar and the dominant angular directions of the impinging field can be estimated. In GPR applications, instead, targets can be present both in the far-field region and near to the antenna. In order to work with DoA algorithms in near-field conditions, we adopted a Sub-Array Processing (SAP) approach [19]: a B-scan is partitioned in sub-radargrams composed of few A-scans each, and the dominant DoA is predicted for each sub-radargram. This method allows to correctly estimate DoAs due to objects that are in the near field of the whole array, as long as they are in the far field of each sub-array. Then, all the estimated angles are triangulated and a set of crossings is obtained, with intersections condensed around object locations. This pattern is filtered, in order to remove the noisy background of unwanted crossings. Finally, the number of targets and their positions are estimated.
- DoA algorithms are conceived by considering a monochromatic or narrowband signal model. They are based on the assumption that the radar is dwelling for a long time on a standing target, gathering the energy in a narrow spectrum of frequencies. Even though this ideal model is adopted in many practical systems (e.g. pulse Doppler radar), the narrowband assumption is too limitative for the GPR case and would lead to a poor spatial localization capability. Moreover, it would impact on the possibility to detect multiple objects. GPR radargrams contain multi-frequency information about the surveyed scenario, which is definitely worth being exploited. Here resides the most innovative part of our method, which takes into account that the radar emits an ultra-wideband signal and exploits the information contained in the entire spectrum of the received signal. In particular, for target-depth estimation (which is more challenging, compared to the estimation of the horizontal position of the target), the matched filter technique is applied [23]. This technique is well known and widely used in other radar applications (such as pulse-doppler, frequency-modulated continuous-wave, and synthetic-aperture radar). However, it does not seem to be used for the processing of radargrams measured by pulsed GPR systems, yet. To the best of our knowledge, our work represents the first application of the matched filter technique for GPR signal processing purposes.

We tested the accuracy of our software tool on synthetic radargrams calculated by using the finite-difference time-domain simulator gprMax [24], with very good results [10], [13].

In Section 2, we provide more information about the approach that we developed and implemented. We also describe the merits and limits of the method.

In Section 3, two examples of application and numerical results are presented. In particular, we use SPOT-GPR for processing the synthetic radargrams obtained for two reference scenarios defined within the COST Action TU1208 [25] (concrete cells with reinforcing elements). We also considered modified versions of such scenarios, where we gradually varied the distances between the reinforcing elements. In this way, we could assess how the electromagnetic interactions between the targets influence the accuracy of our method. We compared the results of proposed method against the classical hyperbola estimation based on a Minimum Mean Square Error technique [26].

In Section 4, conclusions are drawn and plans for future work are outlined.

2. Data-processing Approach Implemented in SPOT-GPR 1.0

We developed and implemented a SAP-DoA method that allows detecting target reflections in a GPR radargram and estimating target positions. For the evaluation of horizontal (x) positions (i.e. the target positions along the acquired GPR profile), our method is based on a beamforming on-receive technique for cross-range localization [26]. For the evaluation of vertical (y) positions (i.e. the target burial depths), which is a more challenging task, proposed method is based on the classic matched-filter technique for range estimation [26]. In Fig. 1, a block diagram of the SAP-DoA method implemented in SPOT-GPR 1.0 is presented.

Our approach operates on the amplitudes of the back-scattered electric field. Hence, as a preliminary step, the radargram of the back-scattered field has to be obtained from the radargram under process where the amplitudes of the total electric field are recorded. The radargram of the

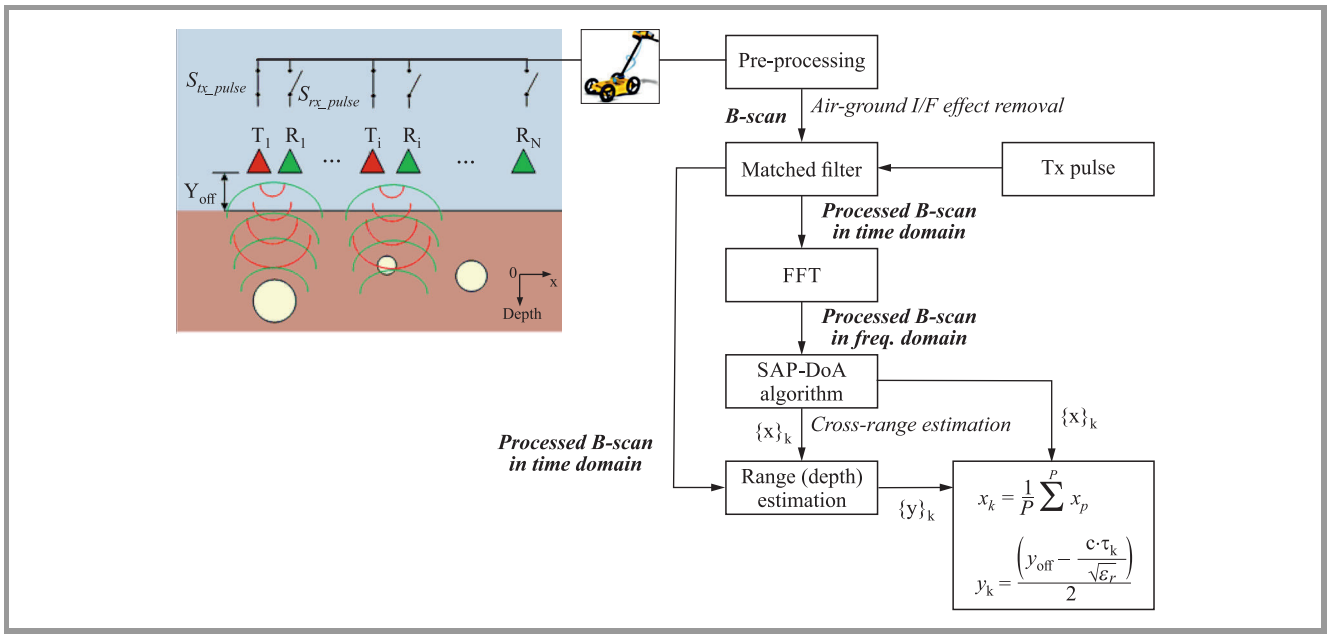

Fig. 1. Block diagram of the signal processing technique implemented in SPOT-GPR 1.0.

back-scattered field can be easily obtained by subtracting a background radargram from the radargram under process. Under the assumption that all the involved media are linear. Let us suppose that the radargram under process includes N A-scans, measured by the GPR in N spatial points along a profile. Then, the background radargram includes N A-scans that would be measured by the GPR in the same spatial points, in the absence of the targets. If the radargram under process is synthetic, the background radargram can be easily produced by using the same electromagnetic simulator that was employed to calculate the radargram under process. If the radargram under process is experimental, an artificial background radargram can be built as follows: the user can select in the B-scan a few traces measured in an area where, for sure, no targets are present (such area has obviously to be far enough from the targets). Then, the selected traces can be averaged and the resulting average trace can be repeated N times.

As was mentioned in the introduction, our approach partitions the radargram of the back-scattered field in sub-radargrams, composed of few traces each. A DoA estimation algorithm is applied to every sub-radargram, for estimating the dominant angle of arrival of the backscattered field. In SPOT-GPR 1.0, the MUSIC algorithm [17] is implemented, which has been widely studied in the literature and is currently the most popular DoA method. Several other high-resolution DoA methods exist. We intend to implement them in the near future and carry out a comparison of their performance when embedded in our approach and applied to GPR scenarios.

By triangulating all the estimated angles, a pattern of intersections (crossings) is obtained. Such intersections are condensed around object locations. The pattern is filtered, in order to remove the noisy background of unwanted crossings [19], [20]. The number of targets and their cross-range (horizontal) positions are estimated by averaging clustered crossings.

DoA algorithms account for a narrowband signal model: they are based on the assumption that the radar is dwelling for a long time on a standing target, gathering the energy in a limited frequency spectrum. Despite this ideal model is used in many practical systems (e.g. pulse Doppler radar), the narrowband assumption is too limitative for the GPR case and would lead to a poor spatial resolution in the vertical direction (the estimation of the target burial depths is more critical than the estimation of their position along the acquisition profile) [8], [9]. Hence, for range estimation, proposed methods adopts the classical matched filter. This technique is widely used in many radar applications but, surprisingly, it does not seem to be used for the processing of GPR radargrams, yet. We carried out a series of tests and the benefits of having integrated this technique into our SAP-DoA approach are significant, in terms of accuracy [10]. Let us call $\{x\}_k$ the set of horizontal coordinates of the intersections in the filtered crossing pattern (with k=1,...,K, being K the number of intersections in the filtered crossing pattern). For each $x_k \in \{x\}_k$, the nearest A-scan is cross-correlated in the time domain with the transmitted pulse. The time instant corresponding to the maximum of the correlated signal $\tau_{obj,k}$ is used to extract the y-coordinate y_k for the k-th crossing. Finally, the position $(\hat{x}_{obj},\hat{y}_{obj})$ of each target is estimated by a simple coordinate averaging of all the $\{x,y\}_k$ pairs located in an area selected by the user via the software GUI.

Let us now underline the main differences between the method implemented in SPOT-GPR, presented in this paper, and a SAP-DoA approach that we proposed and implemented a few years ago. In [19]–[22], the considered scenario was a dielectric lossless half-space hosting circular-section cylindrical targets. The electromagnetic source was

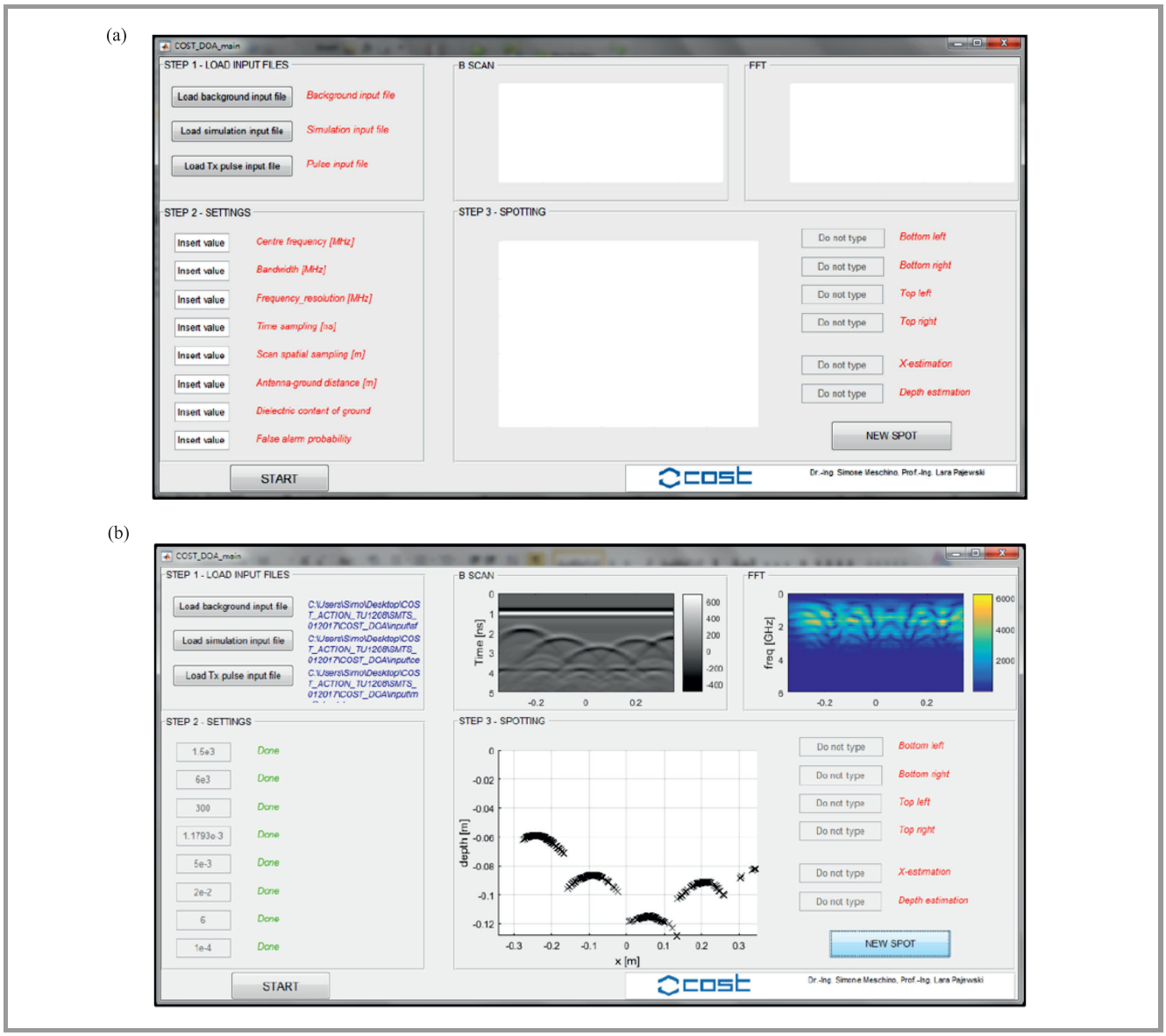

Fig. 2. Layout of the GUI of SPOT-GPR 1.0: (a) screenshot of the input GUI, (b) screenshot of the output GUI.

a monochromatic plane-wave. Spectral-domain results, calculated at a fixed frequency by using the Cylindrical Wave Approach [27], [28], were used as input data for the SAP-DoA method. The old SAP-DoA, indeed, was conceived by considering a monochromatic-signal model. The localization results were satisfactory in the case of one circular-section cylinder and for moderate dielectric contrast between the air and the half-space hosting the target [19]–[21]. The performance of the approach degraded when two interacting cylinders were present, or when the relative permittivity of the soil was increased [22]. The method was not applicable in the presence of more than two cylinders (unless they were very far from each other), because it could not tackle with their electromagnetic interaction. Furthermore, the implemented codes needed a-priori information about the number of sought targets.

The method developed in the framework of the COST Action TU1208 and implemented in SPOT-GPR is more advanced and reliable. It is capable to deal with real GPR radargrams. No a-priori information about the number of targets is needed. Multiple interacting objects, of different size and shape, can be present in the scenario. The electromagnetic source is assumed to be an ultra-wideband signal. The software receives in input the time-domain response of the scenario, measured by the GPR receiving antenna, and is capable to exploit the multi-frequency information contained in it.

The main limitations of SPOT-GPR (release 1.0) are:

- a-priori information is needed concerning the relative permittivity of the medium hosting the targets,
- the method assumes that the medium hosting the target is the medium illuminated by the GPR antenna, i.e. the presence of different media can be taken into account, however they have to be beyond the medium

hosting the targets and not in between such medium and the antennas,

- a-priori information is needed concerning the time-shape of the pulse emitted by the GPR, for the application of the matched-filter technique,
- losses in the media are not taken into account.

We are keen to further develop our method in order to remove those limitations in the near future.
We would like to point out that, commonly, the processing of GPR data for target detection and localization consists in analyzing the hyperbolic reflections found in the radargram. When the electromagnetic pulse emitted by a GPR impinges on a circular-section target embedded in a host medium, the field is scattered and reflected by the target due to the discontinuity of permittivity. As is well known, when the GPR antenna is shifted along the surface between the air and the investigated subsoil/structure, the presence of a circular-section target translates into the recorded radargram as a hyperbola. However, if the target does not have a circular section, its signature in the radargram is not a hyperbola. Hence, the application of the classical hyperbola method for the estimation of its position gives inaccurate results or cannot be applied. Our SAP-DoA approach, instead, is applicable and successful also in the presence of arbitrary-section targets [10].
As mentioned in the introduction, SPOT-GPR 1.0 comes with a GUI. To give an idea, screenshots of the GUI are presented in Fig. 2.
When the software is launched, the graphical interface shown in Fig. 1a appears. This is divided into three main sections, corresponding to three steps to be done by the user in order to obtain the estimation of target positions, namely:

- Step 1 – Load input files: the user is required to select the relevant input files (containing the time shape of the pulse transmitted by the GPR and the data to be processed);
- Step 2 – Settings. The user is required to encode information about some GPR settings used during the measurement;
- Step 3 – Spotting. After the software is executed, the user will be able to interactively drag the mouse on the figure that will appear in the spotting area, in order to extract the estimated positions of the targets.

The GUI output is shown in Fig. 2 and includes the following items:

– a grey-scale map of the synthetic or experimental dataset under analysis (B-scan),

– a color map of the Fast Fourier Transform (FFT) of the compressed simulated/measured dataset,

– the spotting interactive panel, where the user can select an area by simply dragging a rectangular region with the mouse. The relevant estimation of the target positioned in the selected area is provided by the software in the dedicated box, on the right.

More details can be found in the software manual.

3. Examples

In this Section, we consider two reference scenarios proposed within the COST Action TU1208, namely the concrete Cells 1-1 and 1-2 designed and studied in [25].
Cell 1-1 hosts five perfectly-conducting (PEC) circular-section reinforcing bars, having different size and placed at different depths with respect to the air/concrete interface: see the sketch reported in Fig. 1a.
Cell 1-2 refers to a more complex scenario, including both conducting and dielectric objects: a PEC rebar, a polyvinyl chloride (PVC) tube filled with air, a PVC tube partially filled with a perfectly-conducting rebar and with air, and finally a steel pipe (see the sketch in Fig. 1b).
The size of both cells is 60×18 cm in the transverse plane, whereas the length of the cells (and of the reinforcing elements) is 100 cm. The cells are positioned on a compacted fill. Note that in both scenarios the targets are very close to each other: strong electromagnetic interactions take place and, although the geometry of the cells is rather simple, accurate target localization from GPR data is not a trivial task.
For each concrete cell, we simulated four additional configurations where we gradually increased the spacing between adjacent objects with a 5-cm step (as indicated on top of Figs. 1a and 1b).
For the original reference scenarios, synthetic radargrams were already available. They were calculated in [25] by using GprMax2D [29], a free electromagnetic simulator implementing the finite-difference time-domain technique. The new version of the simulator, gprMax [24], was not yet available at that time. For the enlarged versions of the cells, it was necessary to perform new simulations.
In all the simulations, the central frequency of the Ricker pulse emitted by the GPR was f_c = 1.5 GHz. The transmitting antenna (a dipole) and the receiving antenna (not modeled) were at 2 cm from the air-concrete interface (Fig. 3). The distance between the antennas was 10 cm. Results were calculated on a time window of 5 ns, by moving the antennas along a line orthogonal to the axes of the scatterers. The distance between consecutive traces was 5 mm and the time sampling respected the Courant stability condition. The relative permittivity of concrete was $\varepsilon_{r,c} = 6$ and its conductivity was σ_c = 0.01 S/m. The relative permittivity of the compacted fill was $\varepsilon_{r,cf}$ = 16 and its conductivity was σ_{cf} = 0.005 S/m.
The input files for the original cells are reported in the following, in order to encourage interested Readers to consider the same cells for a possible testing of their inversion/imaging/processing approaches and a comparison with our results. The input files for the enlarged configurations can be easily derived.

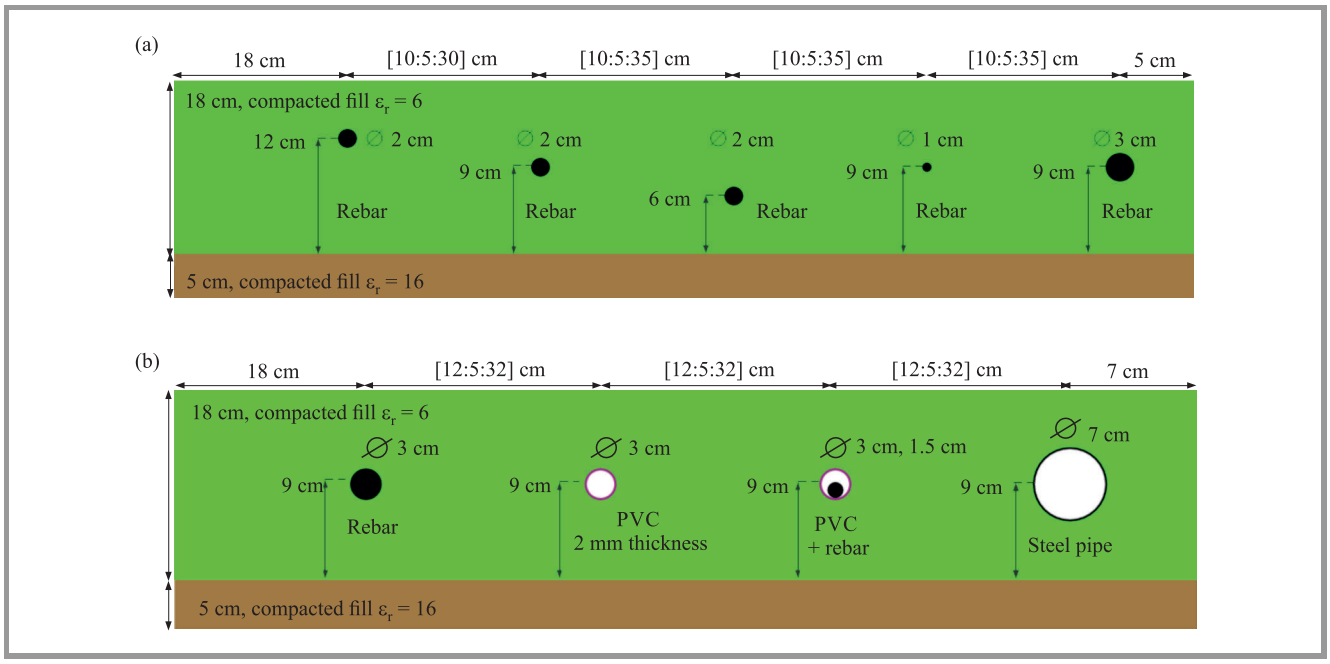

Fig. 3. Test-case geometric model: (a) cell 1-1 – conductive rebars of different size, (b) cell 1-2 – conductive and dielectric objects of different size.

cell_1-1

```
#medium:  6.0 0.0 0.0 0.01 1.0 0.0 concrete
#medium:  16.0 0.0 0.0 0.005 1.0 0.0 compacted_fill
---------------------------------------------------
#domain:  0.66 0.28
#dx_dy:  0.0005 0.0005
#time_window:  5e-9
#abc_type:  pml
#pml_layers:  10
---------------------------------------------------
#box:  0.0 0.0 0.66 0.05 compacted_fill
#box:  0.03 0.05 0.63 0.23 concrete
---------------------------------------------------
#cylinder:  0.18 0.17 0.01 pec
#cylinder:  0.28 0.14 0.01 pec
#cylinder:  0.38 0.11 0.01 pec
#cylinder:  0.48 0.14 0.005 pec
#cylinder:  0.58 0.14 0.015 pec
---------------------------------------------------
#line_source:  1.0 1500e6 ricker MyLineSource
---------------------------------------------------
#analysis:  100 cell_11_concrete.out b
#tx:  0.03 0.25 MyLineSource 0.0 5e-9
#rx:  0.13 0.25
#tx_steps:  0.005 0.0
#rx_steps:  0.005 0.0
#end_analysis:
---------------------------------------------------
#geometry_file:  cell_11_concrete.out.geo
#title:  Cell 1.1
#messages:  y
```

cell_1-2

```
#medium:  6.0 0.0 0.0 0.01 1.0 0.0 concrete
#medium:  16.0 0.0 0.0 0.005 1.0 0.0 compacted_fill
#medium:  3.0 0.0 0.0 0.0 1.0 0.0 pvc
---------------------------------------------------
#domain:  0.66 0.28
#dx_dy:  0.0005 0.0005
#time_window:  5e-9
#abc_type:  pml
#pml_layers:  10
---------------------------------------------------
#box:  0.0 0.0 0.66 0.05 compacted_fill
#box:  0.03 0.05 0.63 0.23 concrete
---------------------------------------------------
#cylinder:  0.18 0.14 0.015 pec

#cylinder:  0.3 0.14 0.015 pvc
#cylinder:  0.3 0.14 0.013 free_space

#cylinder:  0.42 0.14 0.015 pvc
#cylinder:  0.42 0.14 0.013 free_space
#cylinder:  0.42 0.1345 0.0075 pec

#cylinder:  0.54 0.14 0.035 pec
#cylinder:  0.54 0.14 0.033 free_space
---------------------------------------------------
#line_source:  1.0 1500e6 ricker MyLineSource
---------------------------------------------------
#analysis:  100 cell_12_concrete.out b
#tx:  0.03 0.25 MyLineSource 0.0 5e-9
#rx:  0.13 0.25
#tx_steps:  0.005 0.0
#rx_steps:  0.005 0.0
#end_analysis:
---------------------------------------------------
#geometry_file:  cell_12_concrete.out.geo
#title:  Cell 1.2
#messages:  y
```

Table 1
Test scenario for Cell 1-1

Cell 1-1 original			
Object	**Centre position [m]**	**Radius [m]**	**Material**
No. 1	(0.18, 0.17)	0.01	PEC
No. 2	(0.28, 0.14)	0.01	
No. 3	(0.38, 0.11)	0.01	
No. 4	(0.48, 0.14)	0.005	
No. 5	(0.58, 0.14)	0.015	
Size of the cell section: 0.66×0.28 m^2			
No. of A-scans in the radargram: 100			
Cell 1-1 (a)			
Object	**Centre position [m]**	**Radius [m]**	**Material**
No. 1	(0.18, 0.17)	0.01	PEC
No. 2	(0.33, 0.14)	0.01	
No. 3	(0.48, 0.11)	0.01	
No. 4	(0.63, 0.14)	0.005	
No. 5	(0.78, 0.14)	0.015	
Size of the cell section: 0.86×0.28 m^2			
No. of A-scans in the radargram: 140			
Cell 1-1 (b)			
Object	**Centre position [m]**	**Radius [m]**	**Material**
No. 1	(0.18, 0.17)	0.01	PEC
No. 2	(0.38, 0.14)	0.01	
No. 3	(0.58, 0.11)	0.01	
No. 4	(0.78, 0.14)	0.005	
No. 5	(0.98, 0.14)	0.015	
Size of the cell section: 1.06×0.28 m^2			
No. of A-scans in the radargram: 180			
Cell 1-1 (c)			
Object	**Centre position [m]**	**Radius [m]**	**Material**
No. 1	(0.18, 0.17)	0.01	PEC
No. 2	(0.43, 0.14)	0.01	
No. 3	(0.68, 0.11)	0.01	
No. 4	(0.93, 0.14)	0.005	
No. 5	(1.18, 0.14)	0.015	
Size of the cell section: 1.26×0.28 m^2			
No. of A-scans in the radargram: 220			
Cell 1-1 (d)			
Object	**Centre position [m]**	**Radius [m]**	**Material**
No. 1	(0.18, 0.17)	0.01	PEC
No. 2	(0.48, 0.14)	0.01	
No. 3	(0.78, 0.11)	0.01	
No. 4	(1.08, 0.14)	0.005	
No. 5	(1.38, 0.14)	0.015	
Size of the cell section: 1.46×0.28 m^2			
No. of A-scans: 260			
General setup			
Relative dielectric constant medium 1: 6 (concrete)			
Relative dielectric constant medium 2: 16 (compact fill)			
Trace spacing: $5 \cdot 10^{-3}$ m			
Time window: $5 \cdot 10^{-9}$ s			
Centre frequency: 1500 MHz (Ricker pulse)			

Table 2
Test scenario for Cell 1-2

Cell 1-2 original			
Object	**Centre position [m]**	**Radius [m]**	**Material**
No. 1	(0.18, 0.14)	0.015	PEC
No. 2	(0.30, 0.14)	0.015	PVC
	(0.30, 0.14)	0.013	Free space
No. 3	(0.42, 0.14)	0.015	PVC
	(0.42, 0.14)	0.013	Free space
	(0.42, 0.1345)	0.0075	PEC
No. 4	(0.54, 0.14)	0.035	PEC
	(0.54, 0.14)	0.033	Free space
Size of the cell section: 0.66×0.28 m^2			
No. of A-scans in the radargram: 100			
Cell 1-2 (a)			
Object	**Centre position [m]**	**Radius [m]**	**Material**
No. 1	(0.18, 0.14)	0.015	PEC
No. 2	(0.35, 0.14)	0.015	PVC
	(0.35, 0.14)	0.013	Free space
No. 3	(0.52, 0.14)	0.015	PVC
	(0.52, 0.14)	0.013	Free space
	(0.52, 0.1345)	0.0075	PEC
No. 4	(0.69, 0.14)	0.035	PEC
	(0.69, 0.14)	0.033	Free space
Size of the cell section: 0.81×0.28 m^2			
No. of A-scans in the radargram: 130			
Cell 1-2 (b)			
Object	**Centre position [m]**	**Radius [m]**	**Material**
No. 1	(0.18, 0.14)	0.015	PEC
No. 2	(0.40, 0.14)	0.015	PVC
	(0.40, 0.14)	0.013	Free space
No. 3	(0.62, 0.14)	0.015	PVC
	(0.62, 0.14)	0.013	Free space
	(0.62, 0.1345)	0.0075	PEC
No. 4	(0.84, 0.14)	0.035	PEC
	(0.84, 0.14)	0.033	Free space
Size of the cell section: 0.96×0.28 m^2			
No. of A-scans in the radargram: 160			
Cell 1-2 (c)			
Object	**Centre position [m]**	**Radius [m]**	**Material**
No. 1	(0.18, 0.14)	0.015	PEC
No. 2	(0.45, 0.14)	0.015	PVC
	(0.45, 0.14)	0.013	Free space
No. 3	(0.72, 0.14)	0.015	PVC
	(0.72, 0.14)	0.013	Free space
	(0.72, 0.1345)	0.0075	PEC
No. 4	(0.99, 0.14)	0.035	PEC
	(0.99, 0.14)	0.033	Free space
Size of the cell section: 1.11×0.28 m^2			
No. of A-scans in the radargram: 190			
Cell 1-2 (d)			
Object	**Centre position [m]**	**Radius [m]**	**Material**
No. 1	(0.18, 0.14)	0.015	PEC
No. 2	(0.50, 0.14)	0.015	PVC
	(0.50, 0.14)	0.013	Free space
No. 3	(0.82, 0.14)	0.015	PVC
	(0.82, 0.14)	0.013	Free space
	(0.82, 0.1345)	0.0075	PEC
No. 4	(1.14, 0.14)	0.035	PEC
	(1.14, 0.14)	0.033	free space
Size of the cell section: 1.26×0.28 m^2			
No. of A-scans: 220			
General setup			
Relative dielectric constant medium 1: 6 (concrete)			
Relative dielectric constant medium 2: 16 (compact fill)			
Trace spacing: 5×10^{-3} m			
Time window: 5×10^{-9} s			
Centre frequency: 1500 MHz (Ricker pulse)			

In Tables 1 and 2, the physical and geometrical properties of all the considered cells, as well as the simulation parameters, are resumed.

For each enlarged cell, the relevant synthetic B-scan is presented in Figs. 4 and 5. The B-scans of the original cells can be found in [25] and are not repeated here.

We processed all the simulated radargrams with SPOT-GPR, for detecting and localizing the targets. We compared the results obtained with our software with the results obtained by using the traditional hyperbola-fitting method. In particular, for what concerns the latter method, we implemented a dedicated procedure, as follows.

The coordinates of each hyperbolic signature in a radargram do not perfectly lie on a hyperbola. For any point (x_l, y_l) lying on the curve of maximum amplitude, the error with respect to the best fitting hyperbola can be defined as:

$$e^2 = \sum_{l=1}^{L} \left(1 - \frac{x_l^2}{a^2} - \frac{y_l^2}{b^2}\right), \tag{1}$$

being a and b the best-fitting-hyperbola semi major and semi minor axes, respectively.

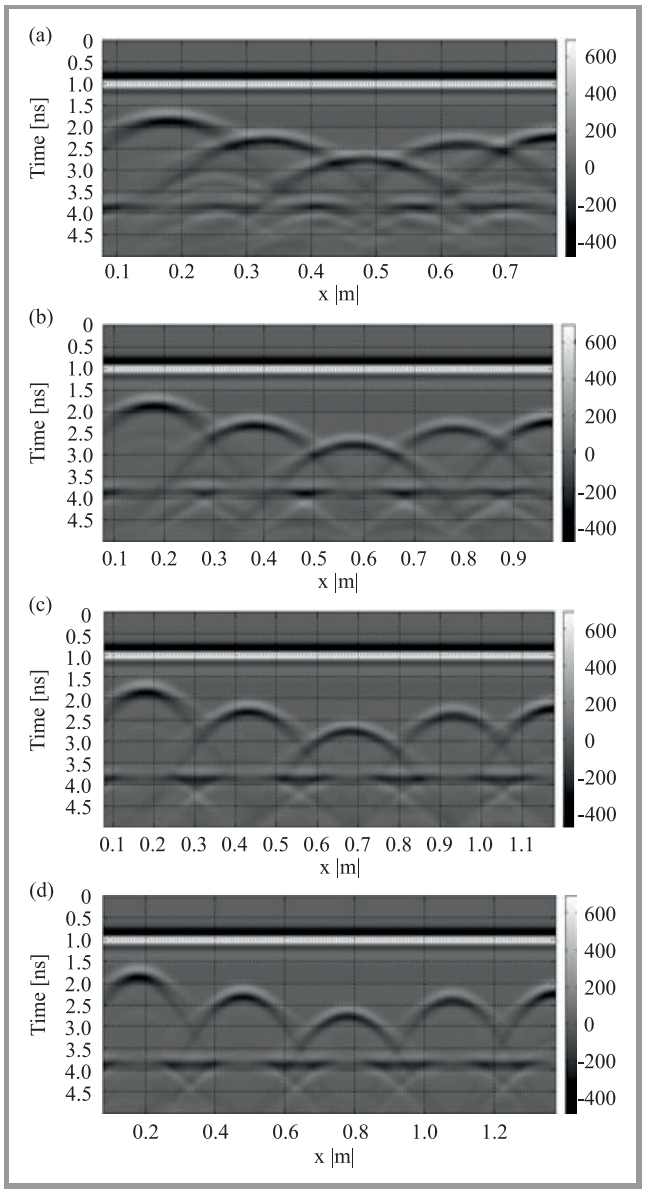

Fig. 4. Radargrams for Cells 1-1 (a)–(d).

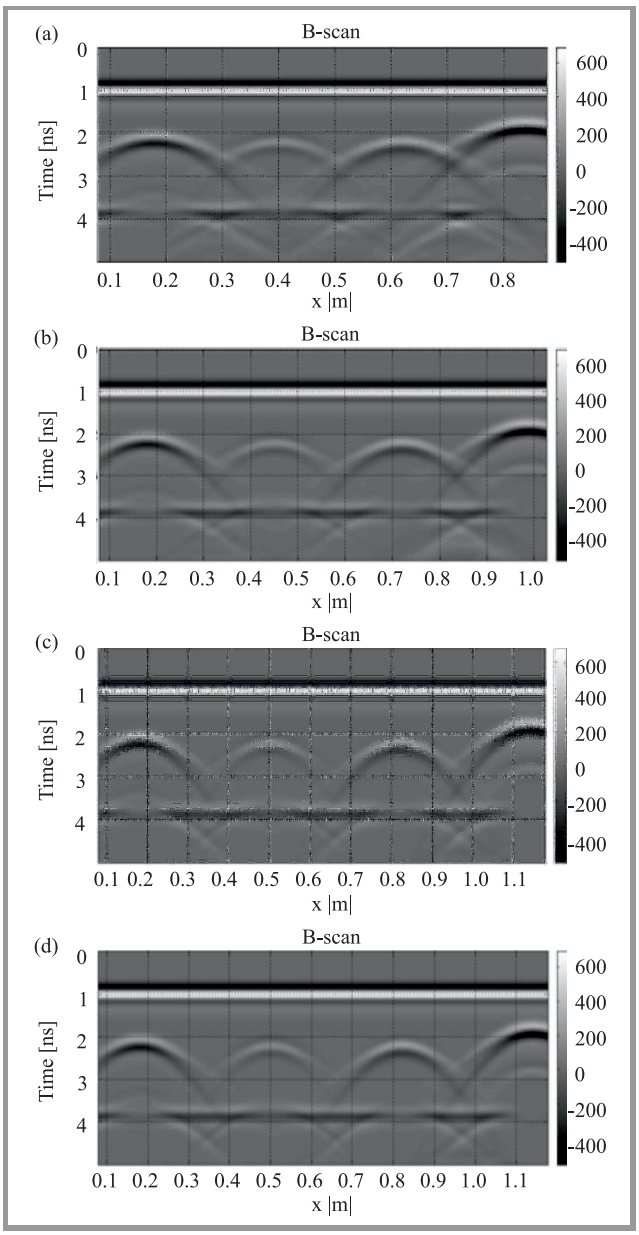

Fig. 5. Radargrams for Cells 1-2 (a)–(d).

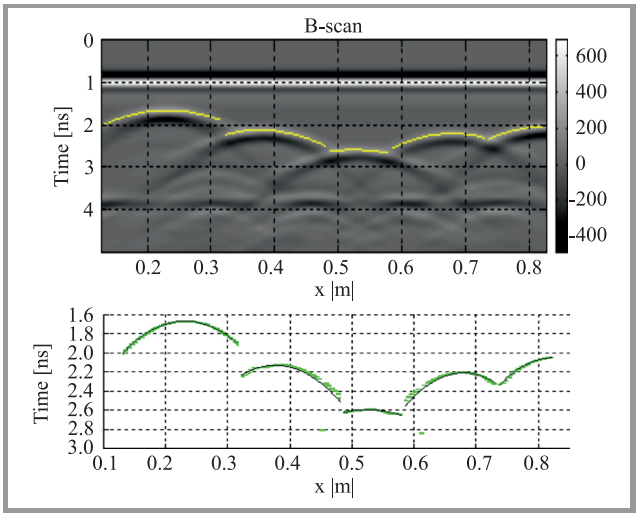

Fig. 6. Hyperbolic data fitting on B-scan data – Cell 1-1 (a).

Table 3
Test results for Cell 1–1

Cell 1–1 original		
Object	**Hyp. position error [m]**	**SAP–DOA position error [m]**
No. 1	(0.0155, –0.0218)	(–0.02, 0.01014)
No. 2	(0.039, –0.0182)	(0.03, 0.0094)
No. 3	(–0.0095, –0.0158)	(–0.0045, 0.005)
No. 4	(–0–009, –0.0146)	(–0.006, 0.0048)
No. 5	(0.007, 0.0143)	(0.02, 0.0114)
Cell 1–1 (a)		
Object	**Hyp. position error [m]**	**SAP–DOA position error [m]**
No. 1	(–0.002, –0.008)	(–0.0174, 0.0104)
No. 2	(0.003, –0.01)	(0.0051, 0.0083)
No. 3	(0.006, –0.011)	(–0.0022, 0.00565)
No. 4	(8.6E–5, –0.005)	(0.0055, 0.00334)
No. 5	(0.007, –0.015)	(0.012, 0.0122)
Cell 1–1 (b)		
Object	**Hyp. position error [m]**	**SAP–DOA position error [m]**
No. 1	(0.0001, –0.008)	(–0.0028, 0.01155)
No. 2	(–0.0012, –0.01)	(–0.0016, 0.009)
No. 3	(0.001, –0.011)	(0.00035, 0.005)
No. 4	(0.0031, –0.005)	(0.0004, 0.004)
No. 5	(0.007, –0.015)	(0.0054, 0.0112)
Cell 1–1 (c)		
Object	**Hyp. position error [m]**	**SAP–DOA position error [m]**
No. 1	(–0.0012, –0.008)	(–0.0018, 0.0286)
No. 2	(–0.003, –0.01)	(–0.0048, 0.0184)
No. 3	(–0.002, –0.011)	(–0.007, 0.005)
No. 4	(0.003, –0.005)	(0.00001, 0.01336)
No. 5	(0.007, –0.015)	(0.001, 0.0142)
Cell 1–1 (d)		
Object	**Hyp. position error [m]**	**SAP–DOA position error [m]**
No. 1	(–0.0063, –0.008)	(–0.008, 0.0294)
No. 2	(–0.0015, –0.01)	(–0.0042, 0.0184)
No. 3	(–0.003, –0.011)	(–0.005, 0.0043)
No. 4	(0.0126, –0.0045)	(–0.005, 0.0135)
No. 5	(0.007, –0.0155)	(0.008, 0.014)

Table 4
Test results for Cell 1-2

Cell 1–2 original		
Object	**Hyp. position error [m]**	**SAP–DOA position error [m]**
No. 1	(–0.0018, –0.0152)	(–0.004, 0.0078)
No. 2	(–0.0033, –0.0248)	(0.0327, 0.0083)
No. 3	(–0.00235, –0.02)	(–0.01, 0.011)
No. 4	(–0.0002, 0.038)	(0.019, 0.0098)
Cell 1–2 (a)		
Object	**Hyp. position error [m]**	**SAP–DOA position error [m]**
No. 1	(–4.72E–4, 0.0149)	(–0.0035, 0.0107)
No. 2	(–0.0018, 0.0054)	(0.001, 0.011)
No. 3	(0.003, 0.0064)	(–0.0036, 0.0171)
No. 4	(2.8E–5, 0.0338)	(0.008, 0.0193)
Cell 1–2 (b)		
Object	**Hyp. position error [m]**	**SAP–DOA position error [m]**
No. 1	(–0.019, 0.00147)	(–0.0025,–0.0126)
No. 2	(0.0951, 0.068)	(–0.001, 0.017)
No. 3	(0.01, 0.059)	(–0.0053, –0.0241)
No. 4	(0.02, 0.038)	(0.0056, 0.026)
Cell 1–2 (c)		
Object	**Hyp. position error [m]**	**SAP–DOA position error [m]**
No. 1	(–0.0043, 0.0148)	(–0.003, 0.0138)
No. 2	(–0.0032, 0.0051)	(–0.0003, 0.0139)
No. 3	(0.0165, 0.0043)	(–0.0022, 0.0139)
No. 4	(–0.0015, 0.0037)	(–0.0003, 0.0241)
Cell 1–2 (d)		
Object	**Hyp. position error [m]**	**SAP–DOA position error [m]**
No. 1	(–0.0127, 0.015)	(–0.003, 0.0134)
No. 2	(0.0015, 0.01)	(–0.0007, 0.0167)
No. 3	(0.003, 0.011)	(–0.003, 0.017)
No. 4	(–0.0126, 0.0045)	(0.00001, 0.008)

The error is therefore a function of the parameters a and b, which have to be estimated by minimizing the square error e^2. The optimal values are obtainable by differentiating e^2 with respect to a and b and by equating the differentials to zero:

$$\begin{cases} \dfrac{\partial e^2}{\partial a} = 0 \\ \dfrac{\partial e^2}{\partial b} = 0 \end{cases}. \tag{2}$$

The latter equation can be solved for a and b and the following expressions can be obtained [26]:

$$a^2 = \frac{\sum_l x_i^4 \sum_l y_i^4 - \left(\sum_l x_i^2 y_i^2\right)^2}{\sum_l x_i^4 \sum_l y_i^2 - \left(\sum_l x_i^2 y_i^2\right) \sum_l x_i^2},$$
$$b^2 = \frac{\left(\sum_l x_i^2 \sum_l y_i^2\right) \sum_l x_i^4 - \left(\sum_l x_i^2 y_i^2\right)^2}{\left(\sum_l x_i^2 y_i^2\right) \sum_l y_i^2 - \sum_l x_i^2 \sum_l y_i^4}. \quad (3)$$

To provide a qualitative idea of the accuracy of such procedure, we present an example in Fig. 6.

The localization results for Cells 1-1 and 1-2 are presented in Tables 3 and 4, respectively. In particular, the position error is given for each target, for both the hyperbolic fitting method and the SAP-DOA technique. The position error is defined as the difference between the actual and estimated positions of the target. It can be noted that the hyperbolic fitting cross-range estimation is pretty close to the SAP-DoA method, whereas the range (depth) estimation of the SAP-DoA method differs from the hyperbolic fitting by less than 2 cm in the worst case. In some cases, the SAP-DoA method is more accurate than the hyperbolic fitting method.

In Fig. 7, the position error is plotted for all the targets of Cell 1-1 and for both localization methods, as a function of the horizontal distance between adjacent targets. Five points are present in each curve. The first point corresponds to the original cell and the subsequent four points correspond to the enlarged cells. In Fig. 8, the same as in Fig. 7 is reported, for Cell 1-2. The SAP-DoA depth-estimation seems to have a little offset in comparison with the hyperbolic fit, which is probably due to the presence of cavities in this case study.

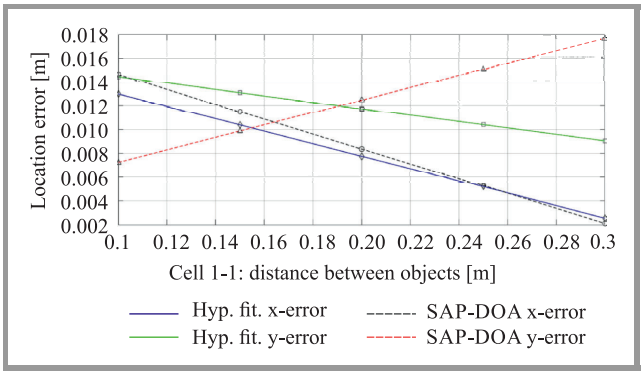

Fig. 7. RMS estimation error vs object mutual distance (5 simulated cases) for Cell 1-1.

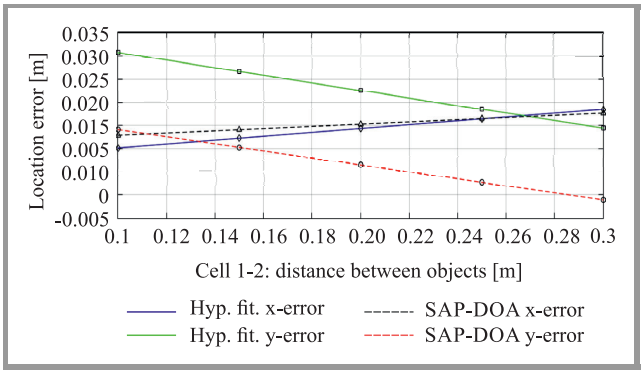

Fig. 8. RMS estimation error vs object mutual distance (5 simulated cases) for Cell 1-2.

4. Conclusions

In this work, an innovative Sub-Array Processing (SAP) approach exploiting Direction of Arrival (DoA) algorithms was presented, for the processing of Ground-Penetrating Radar (GPR) data. The purpose of the method is to detect an unknown number of targets in the subsoil or in a structure, and estimate their positions. For the first time, the matched-filter technique was used in the GPR field, with very good results.

The proposed SAP-DoA approach was developed in the framework of the COST Action TU1208 activities and it was implemented in Matlab. A GUI was realized, too.

The resulting software tool has ben called SPOT-GPR and is freely distributed via the Action website, for academic and commercial use.

The accuracy of the developed tool was investigated by processing several synthetic radargrams, calculated by using the finite-difference time-domain simulator GprMax2D. In this paper we presented two examples. We considered two concrete cells, with embedded metallic and dielectric cylindrical targets. We simulated the cells varying the distance between the targets and processed all the obtained radargrams with SPOT-GPR and compared the obtained localization results with those of the standard hyperbola-fitting approach, which is commonly employed for the processing of GPR data when circular-section cylindrical targets are present. The SAP-DoA technique demonstrated a good functioning with respect to the hyperbolic approach. One of the advantages of our method is that it can be applied also in the presence of arbitrary-section targets, when the hyperbolic fitting method cannot be used.

Further tests will be carried out on synthetic radargrams obtained by including in the model a realistic representation of the transmitting and receiving antennas. Moreover, we will check how the presence of losses in the materials affects the accuracy of our approach.

Additional tests based on real measurements will be carried out. In particular, as a subsequent step, we plan to check the accuracy of SPOT-GPR against the TU1208 experimental dataset coming from measurements performed at the IFSTTAR Geophysical Test Site (Nantes, France) by using several different GPR systems and antennas.

We also plan to implement in our tool different DoA algorithms and compare their performance when applied to GPR scenarios (currently, the tool uses the well-known MUSIC) method.

Acknowledgements

The tool presented in this paper was developed during three COST (European COoperation in Science and Technology) Short-Term Scientific Missions and is a contribution to the COST Action TU1208 "Civil engineering applications of Ground Penetrating Radar". The authors are grateful to COST for funding and supporting the Action TU1208.
This paper is included in the JTIT Special Issue "Recent Progress in Electromagnetic Theory and its Applications" organized by the COST Action TU1208.

References

[1] A. Benedetto and L. Pajewski, Eds., *Civil Engineering Applications of Ground Penetrating Radar*. Book Series: "Springer Transactions in Civil and Environmental Engineering". Springer International Publishing Switzerland, 2015.

[2] R. Persico, *Introduction to Ground Penetrating Radar: Inverse Scattering and Data Processing.* Hoboken, NJ, USA Wiley, 2014.

[3] L. Mertens, R. Persico, L. Matera, and S. Lambot, "Automated detection of reflection hyperbolas in complex GPR images with no a priori knowledge on the medium", *IEEE Trans. of Geosci. and Remote Sensing*, vol. 54, no. 1, pp. 580–596, 2016 (doi: 10.1109/TGRS.2015.2462727).

[4] F. Sagnard, C. Norgeot, X. Derobert, V. Baltazart, E. Merliot, F. Derkx, and B. Lebental, "Utility detection and positioning on the urban site Sense-City using Ground-Penetrating Radar systems", *Measurement*, vol. 88, pp. 318–330, 2016 (doi: 10.1016/j.measurement.2016.03.044).

[5] A. Ristić, Ž. Bugarinović, M. Govedarica, L. Pajewski, and X. Derobert, "Verification of algorithm for point extraction from hyperbolic reflections in GPR data", in *Proc. 9th Int. Worksh. on Adv. Ground Penetrat. Radar IWAGPR 2017*, Nantes, France, 2017, pp. 1–5 (doi: 10.1109/IWAGPR.2017.7996109).

[6] A. Ristić, M. Vrtunski, M. Govedarica, L. Pajewski, and X. Derobert, "Automated data extraction from synthetic and real radargrams of district heating pipelines", in *Proc. 9th Int. Worksh. on Adv. Ground Penetrat. Radar IWAGPR 2017*, Nantes, France, 2017, pp. 1–5 (doi: 10.1109/IWAGPR.2017.7996046).

[7] L. Pajewski, A. Benedetto, X. Derobert, A. Giannopoulos, A. Loizos, G. Manacorda, M. Marciniak, C. Plati, G. Schettini, and I. Trinks, "Applications of Ground Penetrating Radar in civil engineering – COST Action TU1208", in *Proc. 7th Int. Worksh. on Adv. Ground Penetrat. Radar IWAGPR 2013*, Nantes, France, 2013, pp. 1–6 (doi: 0.1109/IWAGPR.2013.6601528).

[8] S. Meschino and L. Pajewski, "Application of a SAP-DoA Method to GPR data, for the Localisation of Scatterers in Concrete", in *Short Term Scientific Missions – Year 2*, COST Action TU1208, L. Pajewski, M. Marciniak, S. Lambot, Eds. Aracne Editrice, Rome, Italy, 2015 [Online]. Available: www.GPRadar.eu

[9] S. Meschino and L. Pajewski, "Application of a SAP-DoA method to GPR data for the location of reinforcing elements in concrete", in *Proc. IEEE 15th Mediterranean Microwave Symp MMS 2015*, Lecce, Italy, 2015, pp. 1–4 (doi: 10.1109/MMS.2015.7375408).

[10] S. Meschino and L. Pajewski, "A study of the accuracy of the SAP-DoA location technique applied to GPR data and comparison with the standard hyperbola approach", in *Short Term Scientific Missions – Year 3*. Aracne Editrice, Rome, Italy, 2017.

[11] L. Pajewski, A. Giannopoulos, S. Lambot, M. Marciniak, S. Meschino, N. Pinel, M. Sbartai, and C. Warren, "Short-term scientific missions on electromagnetic modelling and inversion techniques for ground penetrating radar – COST Action TU1208", in *Proc. 10th IEEE Eur. Conf. on Antennas and Propag. EuCAP 2016*, Davos, Switzerland, 2016 (doi: 10.1109/EuCAP.2016.7482011).

[12] S. Meschino, L. Pajewski, and M. Marciniak, "Development of SAP-DoA techniques for GPR data processing within COST Action TU1208", Geophysical Research Abstracts, European Geosciences Union (EGU) General Assembly 2016, 17-22 April 2016, Vienna, Austria, article ID EGU2016-12565.

[13] S. Meschino and L. Pajewski, "Finalization of a freeware data-processing tool implementing the SAP-DoA technique", in *Short Term Scientific Missions – Year 4*. Aracne Editrice, Rome, Italy, 2017.

[14] L. Pajewski, A. Giannopoulos, M. Marciniak, S. Meschino, A. Popov, I. Prokopovich, A. Ventura, and C. Warren, "Short-Term Scientific Missions on forward and inverse electromagnetic-scattering techniques for Ground Penetrating Radar", in *Proc. Int. Applied Comput. Electromag. Society Symp. ACES 2017*, Florence, Italy, 2017.

[15] B. Gross, *Smart Antennas for Wireless Communications*. New York, NY: McGraw-Hill, 2005.

[16] S. Chandran, *Advances in Direction-of-Arrival Estimation*. Norwood, MA: Artech House, 2005.

[17] R. Kumaresan and D. W. Tufts, "Estimating the angles of arrival of multiple plane waves", *IEEE Trans. on Aerosp. and Electron. Syst.*, vol. 19, no. 1, pp. 13–139, 1983.

[18] R. Roy and T. Kailath, "ESPRIT-estimation of signal parameters via rotational invariance techniques", *IEEE Trans. on Acoust., Speech, and Sig. Process*., vol. 37, no. 7, pp. 984–995, 1989.

[19] S. Meschino, L. Pajewski, and G. Schettini, "Use of a sub-array statistical approach for the detection of a buried object", *Near Surface Geophys.*, vol. 8, no. 5, pp. 365–375, 2010 (doi: 10.3997/1873-0604.2010031).

[20] S. Meschino, L. Pajewski, and G. Schettini, "A direction-of-arrival approach for the subsurface localization of a dielectric object", *J. of Appl. Geophys.*, vol. 85, pp. 68–79, 2012 (doi: 10.1016/j.jappgeo.2012.07.002).

[21] S. Meschino, L. Pajewski, M. Pastorino, A. Randazzo, and G. Schettini, "Detection of subsurface metallic utilities by means of a SAP technique: Comparing MUSIC- and SVM-based approaches", *J. of Applied Geophys*., vol. 97, pp. 60–68, 2013 (doi: 10.1016/j.jappgeo.2013.01.011).

[22] S. Meschino, L. Pajewski, and G. Schettini, "A SAP-DOA method for the localization of two buried objects", *Int. J. on Antenn. and Propag*., vol. 2013, Article ID 702176, 2013 (doi: 10.1155/2013/702176).

[23] C. E. Cook and M. Bernfeld, *Radar Signals: An Introduction to Theory and Application*, 1st ed. Artech House Radar Library, 1993.

[24] C. Warren, A. Giannopoulos, and I. Giannakis, "gprMax: Open source software to simulate electromagnetic wave propagation for Ground Penetrating Radar", *Computer Phys. Commun*., vol. 209, pp. 163–170, 2016 (doi: 10.1016/j.cpc.2016.08.020).

[25] L. Pajewski and A. Giannopoulos, "Electromagnetic modelling of Ground Penetrating Radar responses to complex targets", in *Short Term Scientific Missions and Training Schools – Year 1*, COST Action TU1208, L. Pajewski and M. Marciniak, Eds. Aracne Editrice, Rome, Italy [Online]. Available: www.GPRadar.eu

[26] Bello. Y. Idi and Md. N. Kamarudin, "Utility mapping with Ground Penetrating Radar: an innovative approach", *J. of American Sci.*, vol. 7, no. 1, pp. 644–649, 2011.

[27] M. Di Vico, F. Frezza, L. Pajewski, and G. Schettini, "Scattering by a finite set of perfectly conducting cylinders buried in a dielectric half-space: a spectral-domain solution", *IEEE Trans. on Antenn. and Propag.*, vol. 53, no. 2, pp. 719–727, 2005 (doi: 10.1109/TAP.2004.841315).

[28] M. Di Vico, F. Frezza, L. Pajewski, and G. Schettini, "Scattering by buried dielectric cylindrical structures", *Radio Science*, vol. 40, no. 6, RS6S18, 2005 (doi: 10.1029/2004RS003182).

[29] A. Giannopoulos, "Modelling ground penetrating radar by GprMax", *Construction and Build. Mater*., vol. 19, pp. 755–762, 2005.

Simone Meschino received the M.Sc. degree in Electrical Engineering from the Roma Tre University of Rome, Italy, in 2008. In 2010, he received the Italian engineering qualification and in 2011 the Ph.D. degree at the Roma Tre University of Rome on applied electromagnetics. In 2012 he joined the former Selex ES (nowadays Leonardo Finmeccanica) as radar system engineer then he moved to the former Astrium GmbH (now Airbus Defence and Space, Friedrichshafen, Germany) where he has been working since 2014. His research interests are mainly related to radar topics (including GPR and SAR), in particular sensor array processing, modeling and performance assessment.

E-mail: simone.meschino@gmail.com
Airbus Defence and Space GmbH
a Claude-Dornier-Straße
88090 Immenstaad am Bodensee
Germany

Lara Pajewski – for biography, see this issue, p. 29.